THE JOURNAL OF PHYSICAL CHEMISTRY C
A JOURNAL OF THE AMERICAN CHEMICAL SOCIETY

pubs.acs.org/JPCC
Article

In Situ X-ray Absorption Spectroscopy Study of the Deactivation Mechanism of a Ni-$SrTiO_3$ Photocatalyst Slurry Active in Water Splitting

Published as part of The Journal of Physical Chemistry C special issue "Spectroscopic Techniques for Renewable Energy".

MemetTursun Abudukade,[#] Marco Pinna,[#] Davide Spanu, Giuditta De Amicis, Alessandro Minguzzi, Alberto Vertova, Sandro Recchia, Paolo Ghigna, Guido Mul, and Marco Altomare*

Cite This: https://doi.org/10.1021/acs.jpcc.4c04688

ABSTRACT: We used in situ X-ray absorption spectroscopy (XAS) to investigate the composition−performance correlation of Ni-$SrTiO_3$ photocatalysts active for water splitting. After preparation and exposure to ambient conditions, the Ni particles on $SrTiO_3$ consist of Ni(0) and Ni(II) phases, with a 4:1 at % ratio, in a metal/oxide core/shell configuration, as confirmed by XPS and TEM-EDX. In situ XAS experiments using an aqueous slurry of the Ni-$SrTiO_3$ photocatalyst and simultaneous continuous exposure to 365 nm light with a power density of 100 mW cm^{-2} and the X-rays do not reveal significant changes in oxidation state of the Ni particles. Contrarily, when the X-rays are discontinuously applied, UV excitation leads to oxidation of a significant fraction of Ni(0) to Ni(II), specifically to NiO and $Ni(OH)_2$ phases, along with cocatalyst restructuring. Ni dissolution or oxidation to higher valence states (e.g., Ni(III)) was not observed. The UV light-induced oxidation of Ni(0) causes the hydrogen evolution rate to drop to similar rates as observed for pristine $SrTiO_3$, suggesting that Ni(0) is the active phase for H_2 generation. Our results underscore the importance of assessing the effects of (continuous) X-ray exposure to (photo)catalyst-containing aqueous slurries during in situ XAS experiments, which can significantly influence the observation of compositional and structural changes in the (photo)catalysts. We ascribe this to X-ray induced water photolysis and formation of free electrons, which in this study quench $SrTiO_3$ photoholes and prevent Ni oxidation.

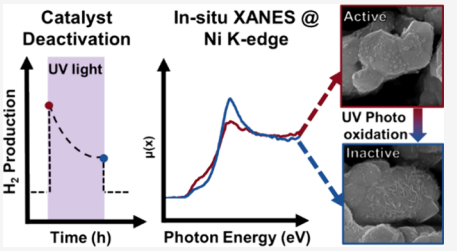

INTRODUCTION

In heterogeneous photocatalysis, semiconductors such as metal oxides are commonly used to absorb UV−visible light and generate charge carriers, i.e., conduction band (CB) electrons and valence band (VB) holes. Once separated, photogenerated charge carriers diffuse toward the surface of the photocatalyst, where they participate in redox reactions.[1−4] Strontium titanate ($SrTiO_3$, herein STO) is one of the most studied photocatalysts in photocatalytic water splitting due to its stability under illumination in aqueous electrolytes and suitable band edge positions that allow for both water reduction to H_2 and water oxidation to O_2.[5] However, bare STO exhibits poor photocatalytic activity, likely due to sluggish kinetics of charge carrier transfer at the semiconductor/electrolyte interface. To overcome this issue, cocatalysts are typically deposited on the surface of semiconductors.[6,7] Noble metals are considered benchmark cocatalysts for proton or water reduction (e.g., Pt or Rh) and their oxides for oxidation of water (e.g., Ru or Ir oxides).[8−10] However, their scarcity and high cost have directed research toward alternative earth-abundant metals.[11−13] Among these, Ni-based materials are an attractive option.[14−17] In alkaline electrolysis, Ni is an efficient catalyst for the hydrogen evolution reaction (HER),[18,19] while NiOOH is active for the oxygen evolution reaction (OER).[20,21]

STO photocatalysts, surface-modified with various Ni-based cocatalysts, have been widely investigated in the last decades.[15,17,22−26] Earlier studies applying a relatively long time resolution (hours) for analysis of H_2 and O_2 evolution[25] reveal little changes in performance over time, while recent studies applying gas chromatography with minute-time resolution and ppm-level detectors reveal significant changes in H_2 evolution rate and H_2:O_2 ratio in the first hour(s) of exposure to UV illumination.[15,16]

The function of the NiO shell in NiO/Ni particles, present after preparation of the catalyst, was proposed by Domen et al. to promote the HER, with the metallic Ni core providing ohmic

Received: July 15, 2024
Revised: September 5, 2024
Accepted: September 9, 2024

contact and hence electron transfer from STO to the NiO shell.[22] It was also proposed by the same authors that water oxidation is catalyzed by the free STO surface.[22] On the contrary, Baba and Fujishima proposed that the cathodic site for hydrogen evolution is the bare STO surface.[27] Finally, Townsend and colleagues suggested that in NiO/Ni-STO photocatalysts, Ni is the HER catalyst, and NiO the OER site.[17] In most of these studies, the Ni-STO photocatalysts were photoexcited using simulated solar light and, hence, with relatively low UV photon fluxes.

Structural changes in the NiO/Ni particles have also been observed on the shorter time scales of light exposure (<1 h) and have been correlated with changes in performance. Zhang et al. reported on deactivation of the photocatalyst and assigned this to a photoinduced oxidation/dissolution of the metallic core in the NiO/Ni cocatalyst, similarly to what was posited by Townsend et al.[16] Han et al. investigated the transient behavior of NiO/Ni-STO under intermittent illumination. They proposed a mechanism based on three redox steps: (i) the light-driven oxidation of surface $Ni(OH)_2$ to trivalent Ni species (NiOOH) and protons (H^+), as reported in eq 1, (ii) proton reduction on metallic Ni sites (eq 2), and (iii) the reaction of NiOOH and Ni to $Ni(OH)_2$ (eq 3) under dark conditions, leading to catalyst regeneration.[15] A more recent study from the same authors shows that deposition of CrO_x improves the stability of the NiO/Ni cocatalyst on Mg-doped STO due to formation of a mixed metal oxide phase ($NiMgCrO_x$), which is proposed to be the active site for HER.[28]

$$Ni(OH)_{2(s)} + h^+_{VB} \rightarrow NiOOH_{(s)} + H^+_{(aq)} \quad (1)$$

$$2H^+_{(aq)} + 2e^-_{CB} \rightarrow H_{2(g)} \quad (2)$$

$$2NiOOH_{(s)} + Ni_{(s)} + 2H_2O_{(l)} \rightarrow 3Ni(OH)_{2(s)} \quad (3)$$

All these propositions for composition and structural changes, however, were based on ex-situ characterization techniques and should be analyzed critically as photocatalysts were exposed to environmental conditions after photocatalysis. Thus, the Ni speciation measured by ex-situ methods (e.g., XPS, XAS) after photocatalysis might not be fully representative of the photocatalyst state during photocatalysis.

Some of us previously used operando X-ray absorption spectroscopy (XAS) techniques to investigate the dynamic behavior of Ni (and Cu) cocatalyst nanoparticles (NP) on TiO_2 in photocatalytic H_2 generation from alcoholic aqueous mixtures.[29] We observed cocatalyst dissolution in the dark (forming Ni^{2+} (aq.) or Cu^{2+} (aq.) species), followed by a UV-light-induced healing of the cocatalyst, i.e., photodeposition onto TiO_2 of metallic Ni or Cu from solvated Ni^{2+} or Cu^{2+} species, causing a gradual increase of the H_2 evolution rate. In the presence of a hole scavenger (i.e., when holes are rapidly consumed), metallic Ni (or Cu) is the active site for H_2 evolution. In a more recent study, simple illumination of slurries of reduced TiO_2 powders in the presence of a dissolved Ni(II) salt was found to form metastable Ni(I) species active toward H_2 generation, as probed by in situ XAS and EPR spectroscopy techniques.[30]

In the present work, we study the composition−performance correlation of a Ni-STO photocatalyst for overall water splitting under UV exposure (365 nm, 100 mW cm^{-2}), in the absence of sacrificial species, focusing on in situ X-ray spectroscopy. For the photocatalytic water splitting tests, we used a continuously stirred tank photoreactor connected to an online gas chromatograph (micro-GC, with PDD), providing a high time resolution of 2 min. We critically assess in situ XAS experiments and demonstrate that X-ray exposure should be minimized to observe UV light-induced composition and structural changes of the Ni-STO photocatalyst. In particular, we reveal oxidation of the metallic Ni phase, within a few hours of UV illumination, to Ni(II) species, namely, NiO and $Ni(OH)_2$ solid phases. Given the concurrent decrease in H_2 evolution rate, we infer that the metallic nickel (Ni(0)) is the cocatalyst phase active for H_2 generation.

METHODS

Preparation of Ni-STO. The Ni-STO photocatalyst was prepared by following a recipe reported in a previous study.[15] STO was synthesized by a high-temperature solid-state synthesis. Stoichiometric amounts of $SrCO_3$ (99.995%, Sigma-Aldrich) and rutile TiO_2 (99.995%, Sigma-Aldrich) were mixed by grinding in an agate mortar for 15 min, placed in a ceramic sample-holder, and calcined at 1000 °C (heating rate 10 °C min^{-1}) for 1 h in static air. To obtain a nominal loading of 3 wt % of Ni cocatalyst NPs on STO, we employed a wet impregnation method using a Ni salt ($NiNO_3 \cdot 6H_2O$) following a recipe previously reported.[31] To do so, 200 mg of synthesized STO powders was dispersed in 20 mL of a 3.95 mM $Ni(NO_3)_2$ aqueous solution and stirred for 2 h. Then, the solution was evaporated in air at 80 °C overnight and transferred into a tube furnace for the following thermal treatment. In the tube furnace, the powders were first calcined at 400 °C in air (30 mL min^{-1}) for 30 min, and then flushed in Ar (50 mL min^{-1}) to cool down to room temperature. After reaching room temperature, the Ar flow was replaced by 5% H_2 in Ar (30 mL min^{-1}) and then the sample was heated to 500 °C for 5 h. The sample was then cooled to room temperature in a flow of Ar. Contrary to earlier studies, the sample was not exposed to a mild oxidation in air at 200 °C but carefully exposed to ambient conditions. Finally, the catalyst powder was ground and stored in a capped glass vial.

Ex-Situ Characterization. The morphology of the Ni-STO photocatalyst powders was examined by field emission scanning electron microscopy (FE-SEM, JEOL, JSM-7610F) and high-angle annular dark-field imaging-transmission electron microscopy (HAADF-TEM, Thermo Scientific Spectra 300 S/TEM). The chemical composition of the cocatalyst was analyzed by energy-dispersive X-ray spectroscopy-transmission electron microscopy (EDX-TEM, Thermo Scientific Spectra 300 S/TEM) and X-ray photoelectron spectroscopy (XPS, PHI Quantes scanning XPS/HAXPES microprobe, Al Kα, 100 μm beam). CasaXPS software (Casa Software, Ltd.) was used for C 1s correction and fitting of the high-resolution Ni 2p spectra. Fitting of the experimental XPS spectra was performed by using Voigt curves and a Shirley background. X-ray diffraction was used to analyze the crystallographic properties of the photocatalyst powders (D2 PHASER, Bruker, Cu Kα source, step size 0.02°, 0.5 s/step, scan range 10−80°). Inductively coupled plasma mass spectrometry (ICP-MS, ICAP Q, Thermo Scientific) was used to evaluate the actual loading of Ni on STO, the molar ratio of Sr and Ti, and to investigate the possibility of Ni dissolution in water during the photocatalytic experiments. 9.97 mg of Ni-STO powders was added in a PTFE vessel along with 5 mL of trace-grade analysis hydrochloric acid (37% v/v, VWR). Microwave-assisted acid digestion was performed under temperature-controlled conditions at 190 °C for 6 h by employing an ETHOS One (Milestone) digestion

https://doi.org/10.1021/acs.jpcc.4c04688
J. Phys. Chem. C XXXX, XXX, XXX−XXX

system. After digestion, the samples were diluted and acidified with ultrapure nitric acid obtained by sub-boiling distillation.[32] 30 g of digested solution was analyzed to determine the Ni loading and molar ratio of Sr and Ti. Photocatalyst suspensions (sampled after suspending the powders in water under dark or illumination conditions) were filtered and stabilized by acidification using nitric acid of trace-grade analysis quality (65%, Suprapur, Supelco). Diluted solutions were analyzed by ICP-MS.

Photocatalytic Experiments. The photocatalytic activity of the Ni-STO powders was measured by using a continuously stirred tank reactor connected to an online gas chromatograph (GC) equipped with a pulsed discharge detector (GC-PDD, CompactGC 4.0, Interscience). See Figure S1 for a scheme and a photograph of the setup. The photoreactor was a gastight system based on an optical glass cuvette (402.013-OG, Hellma). The cuvette was filled with 25 mL of an aqueous catalyst suspension (slurry) with a concentration of photocatalyst of 1 mg mL^{-1} (e.g., 25 mg of Ni-STO in 25 mL of deionized (DI) water). This catalyst concentration is at the upper limit of the linearly increasing regime of the rate as a function of catalyst concentration.[33] To disperse the photocatalysts, 25 mg of catalyst powder was added to 10 mL of DI water in a glass vial. To ensure complete retrieval of the photocatalyst, DI water was added to the glass vial and sonicated. This step was repeated twice up to a total volume of 25 mL. Once loaded in the reactor, the suspension was kept under vigorous stirring and illuminated with monochromatic UV light (LED Control 5S, Opsytec, λ = 365 nm, irradiance = 100 mW cm^{-2}). A constant He flow (10 mL min^{-1}) was bubbled through the suspension first to remove dissolved oxygen in the solution under dark conditions and then, under UV illumination, to purge the gaseous products (H_2 and O_2) to the GC for quantification. The time resolution of the online GC analysis is 2 min, and the response delay is 3 min. The production rate of H_2 and O_2 (μmol h^{-1} g_{cat}^{-1}) is calculated according to eq 4:

$$\text{production rate} = \frac{C_x \times j}{V_M \times m_{cat}} \quad (4)$$

where

- C_x is the concentration of evolved H_2 or O_2 gas expressed as part per million (μL L^{-1})
- j is the flow rate of carrier gas (He) expressed in L h^{-1}
- V_m is the molar volume at 298.73 K (24 μL μmol^{-1})
- m_{cat} is the mass of the catalyst expressed in grams

In Situ XAS Experiments and Spectroscopic Cell Design. The in situ XAS experiments were conducted at beamline P65 (PETRA III storage ring) at DESY, Hamburg, Germany, and at beamline XAFS at ELETTRA, Trieste, Italy. For the in situ XAS experiments, we used a liquid-phase cell as shown in Figure S2a, similar to that used in a previous work.[29] This cell has a thin Mylar front window (01867-AB, SPI, 6 μm) to provide transparency for both X-ray and UV light and is gastight, allowing for online analysis of the gas head space by GC. The photocatalyst suspension, kept under constant stirring, was purged continuously with Ar during the experiments to simulate the photocatalytic conditions adopted with the photocatalytic reactor (Figure S1), including the UV photon flux irradiated on the photocatalyst slurry. We performed in situ experiments in fluorescence mode, while reference samples (metallic Ni, NiO powder, $Ni(OH)_2$ powder, and aqueous $NiSO_4$ solution) and pellets of as-prepared Ni-STO powder were analyzed in transmission mode. X-ray absorption near edge structure (XANES) spectra were collected in the −150 to +150 eV photon energy range with respect to the Ni K-edge (8333 eV), allowing to record one spectrum every ∼3 min and hence to carry out time-resolved experiments. To minimize the effect of beam damage (discussed in Results and Discussion), the exposure of the photocatalyst slurry to the probing X-ray beam was systematically reduced in a series of in situ experiments; while this approach reduced the time resolution, it allowed to follow Ni redox processes caused by UV excitation of Ni-STO. Quantitative analysis of the different Ni species in the cocatalyst was obtained by fitting the acquired spectra using linear combinations of reference spectra with the Athena software.[34]

RESULTS AND DISCUSSION

The morphology of bare STO and Ni-STO particles was analyzed by SEM. The STO powders consist of round-shaped, agglomerated particles in the size range of 100−500 nm (Figure 1a). Upon surface modification of STO, nanoparticles (NPs) of Ni in the size range of 10−30 nm are formed (Figure 1b). The

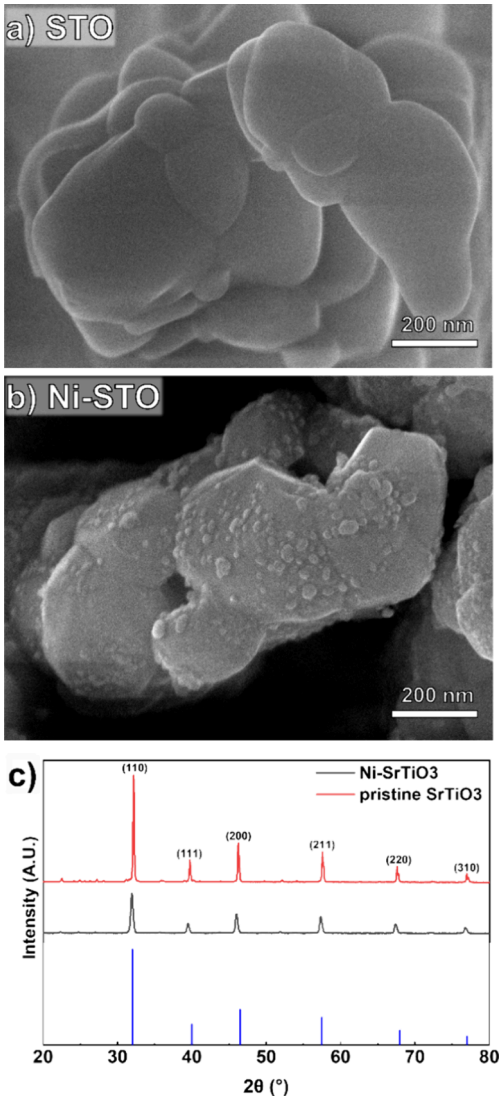

Figure 1. High-resolution SEM images of (a) pristine STO and (b) Ni-STO. (c) XRD patterns of pristine STO and Ni-STO.

https://doi.org/10.1021/acs.jpcc.4c04688
J. Phys. Chem. C XXXX, XXX, XXX−XXX

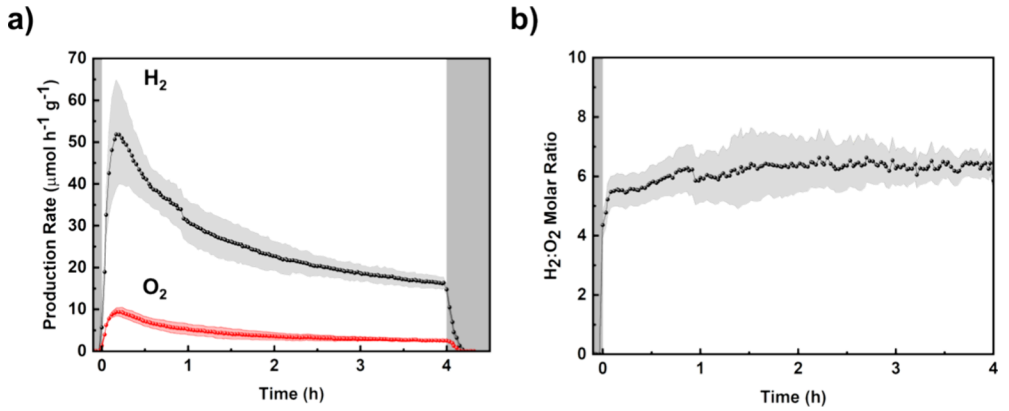

Figure 2. (a) Production rate profiles for H_2 (black) and O_2 (red) during overall photocatalytic water splitting. (b) Molar ratio of evolved H_2 and O_2. The light gray and red shaded areas represent the standard deviation calculated for the same experiment reproduced three times, and the gray and white areas represent times in the absence of UV illumination (dark condition) and UV irradiation steps, respectively.

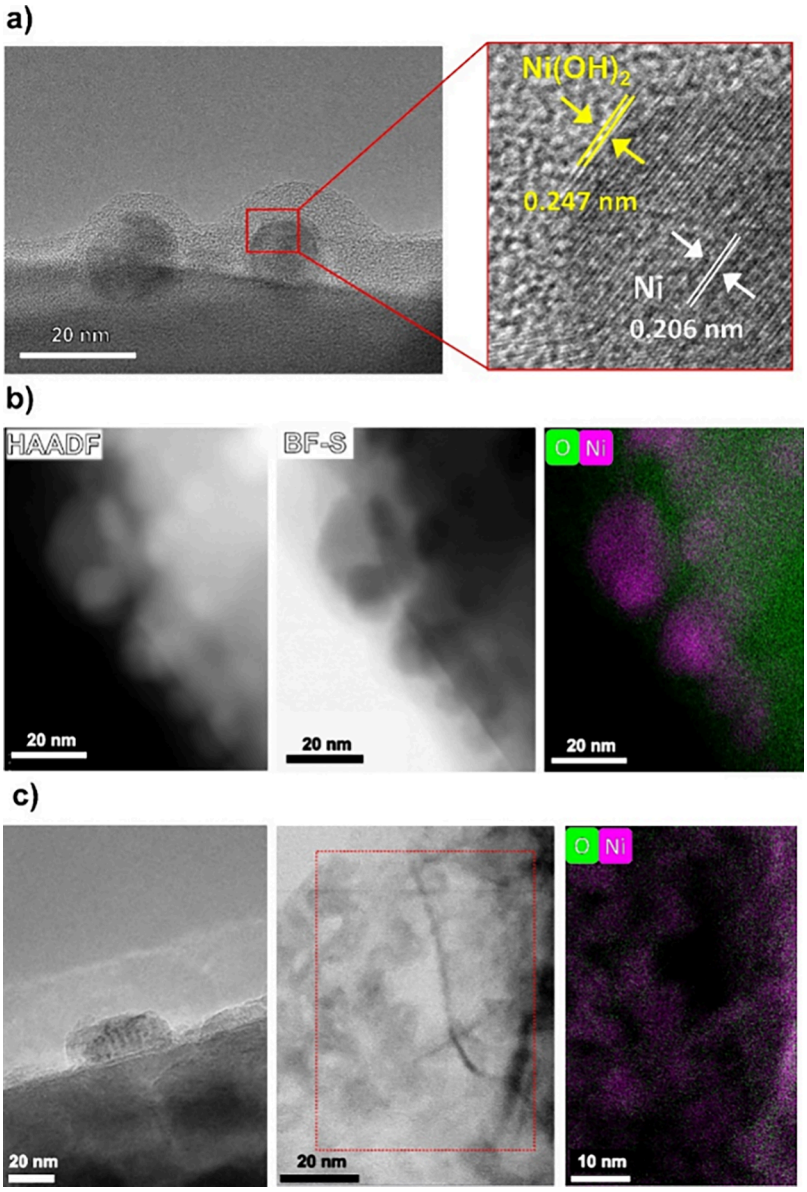

Figure 3. (a, b) As-prepared Ni-STO photocatalyst: (a, left) TEM and (a, right) HR-TEM images; (b, left) HAADF and (b, center) BF-S images; (b, right) TEM-EDX elemental mapping. (c) Ni-STO photocatalyst after 6 h of photocatalysis: (c, left) TEM and (c, center) HR-TEM images and (c, right) TEM-EDX elemental mapping.

https://doi.org/10.1021/acs.jpcc.4c04688
J. Phys. Chem. C XXXX, XXX, XXX−XXX

ICP-MS measurements show a stoichiometric molar ratio between Sr and Ti (Sr:Ti = 1.0) and a 2.0 wt % loading of Ni. The crystalline nature of both pristine STO and Ni-modified STO is confirmed by XRD analysis (see XRD patterns in Figure 1c).[35]

TEM analysis (Figure 3a, to be discussed later) clearly shows that the Ni particles consist of Ni/NiO core−shell particles—similar to a previous study.[15]

The photocatalytic activity of Ni-STO was tested under intermittent, high-UV photon flux illumination (Figure 2). Soon after the UV illumination is switched on, both H_2 and O_2 production rates reached a maximum value of 50 ± 13 and 9 ± 1 μmol h^{-1} g^{-1}, respectively (Figure 2a). This production rate is equivalent to an apparent quantum efficiency of ∼0.2%. This value is significantly lower than values reported in the literature, explained by the high intensity of UV light (100 mW cm^{-2}) entering the reactor, equivalent to values in which the reaction rate likely no longer increases linearly as a function of photon flux. We applied high light intensities to accelerate possible composition and structural changes of the photocatalyst induced by UV light exposure. A continuous decrease in both H_2 and O_2 evolution rates can be observed, just after the peak in production rate is reached—this testifies the rapid photocatalyst degradation under high photon flux UV irradiation.

This, together with the observation that the molar ratio of H_2:O_2 is higher than 2:1 (Figure 2b), suggests that photogenerated holes in Ni-STO take part in other redox processes than just the OER, probably causing oxidation of the cocatalyst. Additional photocatalytic experiments using the same photocatalyst slurry were performed under intermittent UV illumination (light on/off cycles, Figure S3). The deactivation of the catalyst appears to occur in two phases: a relatively fast initial phase, followed by a slower secondary phase. As shown in Figure S3, when UV light is switched on again, after a dark period of 15 h, the hydrogen production rate peaks initially at the same value reached at the end of the first irradiation cycle and then decays in a similar manner. Hence, we can conclude that degradation of the photocatalyst takes place under UV illumination, while the resulting composition of Ni-STO is stable in water under dark conditions. This behavior is different from the study of Han and co-workers on a similar catalyst system,[15] who observed significant recovery of the initial rate after applying a period in the dark—implying that our catalyst does not express the composition and structural changes observed by Han and co-workers.[15]

To reveal composition changes, we initially performed ex-situ TEM analysis. TEM images of the as-prepared sample (Figure 3a) show the core−shell nature of the Ni cocatalyst NPs. The Ni NPs in Figure 3a (left) have a diameter of ca. 10−15 nm (in line with the average NP diameter observed by SEM, Figure 1). The average NP shell thickness is approximately 2 nm (Figure 3a, right). The metallic nature (Ni(0)) of the core was confirmed by analysis of the lattice spacing, i.e., 0.206 nm, attributed to the Ni (111) planes, while the lattice spacing of 0.247 nm observed for the shell can be attributed to the (220) planes of NiO (Ni(II)).[36] Elemental mapping of the NP via TEM-EDS measurements (Figure 3b) shows that both Ni and O are present in regions corresponding to the outer layer (shell) of the cocatalyst NPs, providing further proof of a metal/oxide core−shell structure.

After photocatalysis, Ni NPs with a rougher surface can be observed (Figure 3c), along with the presence of few nanometer-thick flake-like structures, also observable by SEM (below, Figure 4). The TEM-EDS elemental map of the flakes (Figure 3c) shows a homogeneous distribution of Ni and O, suggesting that such nanoflake formations are composed of an oxidized Ni phase, e.g., $Ni(OH)_2$, which is known to grow in sheet/plate-like morphologies.[37]

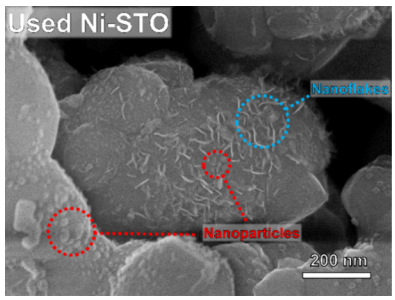

Figure 4. High-resolution SEM (HR-SEM) image of Ni-STO after 6 h of photocatalysis. For ease of visualization, some core−shell NPs have been highlighted in red, while flake-like nanostructures have been highlighted in blue.

XPS measurements for the photocatalyst powders were performed before and after photocatalysis to assess possible changes in the oxidation state of the Ni cocatalyst (Figure 5). The Ni 2p spectra reveal the presence of metallic Ni (at 852.30 eV), NiO (at 854.10 eV), and $Ni(OH)_2$ (at 855.42 eV) phases, attributed to electronic transitions from Ni 2p 1/2 and Ni 2p 3/2 levels, in agreement with previous literature.[38] Quantitative analysis showed that $Ni(OH)_2$ is present as the predominant species in both samples. This could be explained by the nature of XPS: being a surface-sensitive technique, with a probing depth in the nanometer range,[39] only the outer layer of the NP can be probed by XPS (outermost ∼5 nm or so). Although a slight oxidization of metallic Ni after photocatalysis might have taken place (the fraction of $Ni(OH)_2$ on the cocatalyst surface increased from 53 to 62%, Figure 5c), these minor changes cannot fully justify the significant deactivation observed with the photocatalytic measurements (Figure 2). Furthermore, XPS results indicate that cocatalyst dissolution did not take place during photocatalysis, as the surface atomic content of Ni (at%) for the samples before and after photocatalysis is identical within the experimental error of the applied technique (Table S1). These results are corroborated by ICP-MS data (Table S2), showing that suspending photocatalyst powders in DI water for up to 15 h in the dark, or under UV illumination for up to 6.5 h, only leads to dissolution of negligible amounts of nickel (typically in the order or below 0.1% of the Ni mass initially loaded on STO).

The composition of the Ni NP in the as-prepared photocatalyst was also measured by ex-situ XAS measurements. The fitting results show that the cocatalyst is mainly composed of metallic Ni (∼80%, NP core) with a ∼ 20% of Ni(II) phase, in the form of NiO and $Ni(OH)_2$, accounting for the composition of the NP shell (see Figure S4 along with a brief description of the spectral shapes in the Supporting Information).

Most importantly, we performed in situ XAS experiments to investigate in real time changes in the Ni oxidation state during photocatalysis, under high-flux UV irradiation. To achieve temporal resolution in the range of minutes, spectra were acquired only in the XANES region. NiO and $Ni(OH)_2$ phases cannot be easily discriminated by fitting XANES spectra. Thus, phase composition data are provided as the content of metallic Ni (Ni(0)) and Ni(II), where the content of Ni(II) includes both NiO and $Ni(OH)_2$ phases. Analyzing the results using the

https://doi.org/10.1021/acs.jpcc.4c04688
J. Phys. Chem. C XXXX, XXX, XXX−XXX

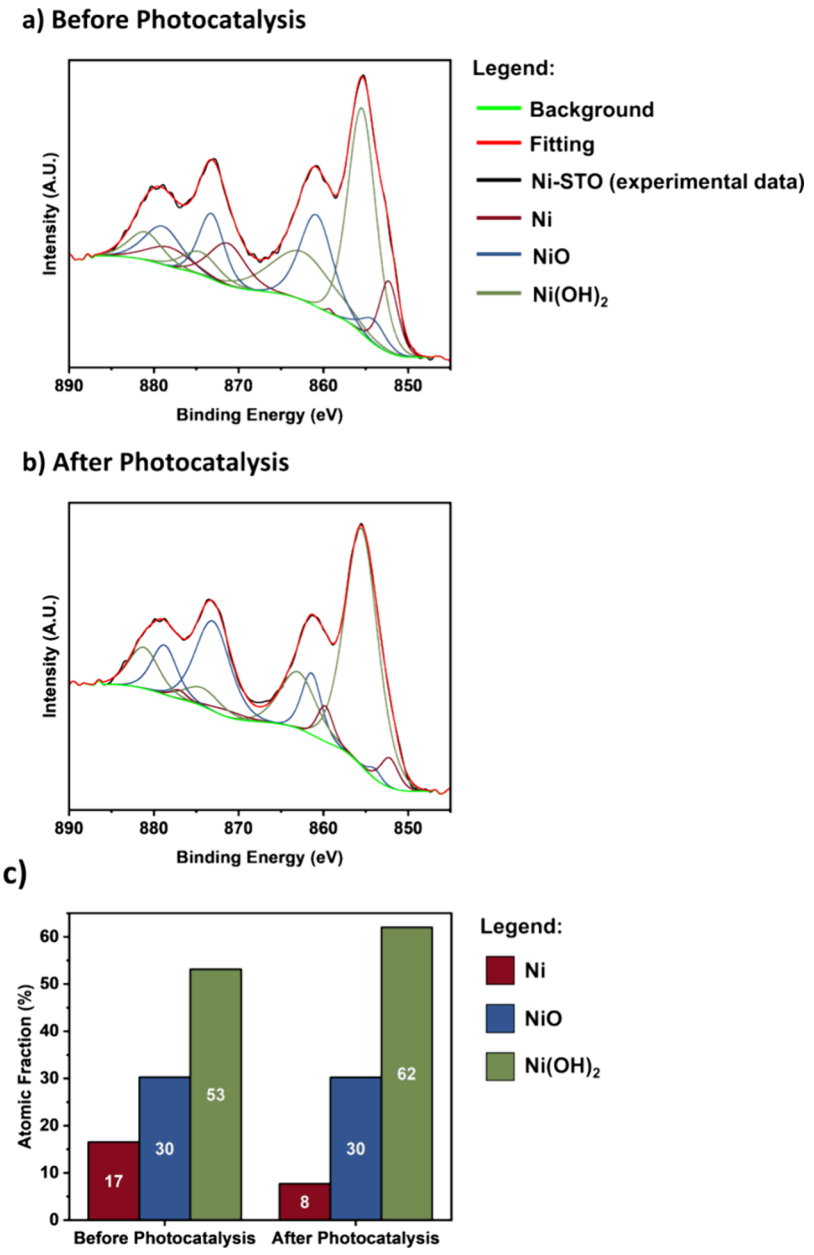

Figure 5. (a, b) Ni 2p HR-XPS spectra for the as-prepared sample and after 6 h of photocatalysis, respectively. (c) Relative surface composition of Ni before and after photocatalysis.

reference spectrum of NiOOH as the fitting component resulted in a lower fitting quality of the in situ spectra (Figure S5). We therefore exclude the presence or formation of Ni(III) phases. Moreover, solvated Ni(II) species were also not identified, indicating no or negligible dissolution of the Ni cocatalyst, well in line with XPS and ICP-MS results.

During preliminary in situ XAS experiments (in DI H_2O, under UV light on−off cycles), only negligible changes in Ni phase composition were observed both in the dark and under UV illumination conditions (Figure S6, discussed in the SI). Online GC analysis of the gas headspace from the in situ XAS cell in the absence of X-rays (Figure S7) provides H_2 and O_2 evolution profiles similar to those measured with the reactor applied in our lab (compare Figure S7 and Figure 2). That is, when UV is switched on, both H_2 and O_2 evolution profiles reach a maximum rate in a few minutes, followed by a rapidly decreasing H_2 evolution rate. Hence, the in situ XAS data in Figure S6 cannot explain the photocatalyst deactivation; the significant decrease in hydrogen production rate and lack of changes in the composition of Ni/NiO core−shell particles are difficult to reconcile.

Therefore, we performed a series of in situ experiments where the UV-illuminated photocatalyst slurry was exposed to the probing X-ray beam (for XAS spectra collection) for gradually shorter times (Figure 6).

In each experiment, prior to UV light illumination, no significant change of the Ni(0) and Ni(II) composition can be observed, the at % ratio remaining close to the initial one of 4:1. Moreover, photocatalytic experiments carried out after different durations of the initial He purging step in the dark show comparable H_2 gas evolution profiles (Figure S8). This further confirms that the photocatalyst is stable in DI water in the dark, and no cocatalyst degradation takes place in the aqueous suspension before or in the absence of UV irradiation.

https://doi.org/10.1021/acs.jpcc.4c04688
J. Phys. Chem. C XXXX, XXX, XXX−XXX

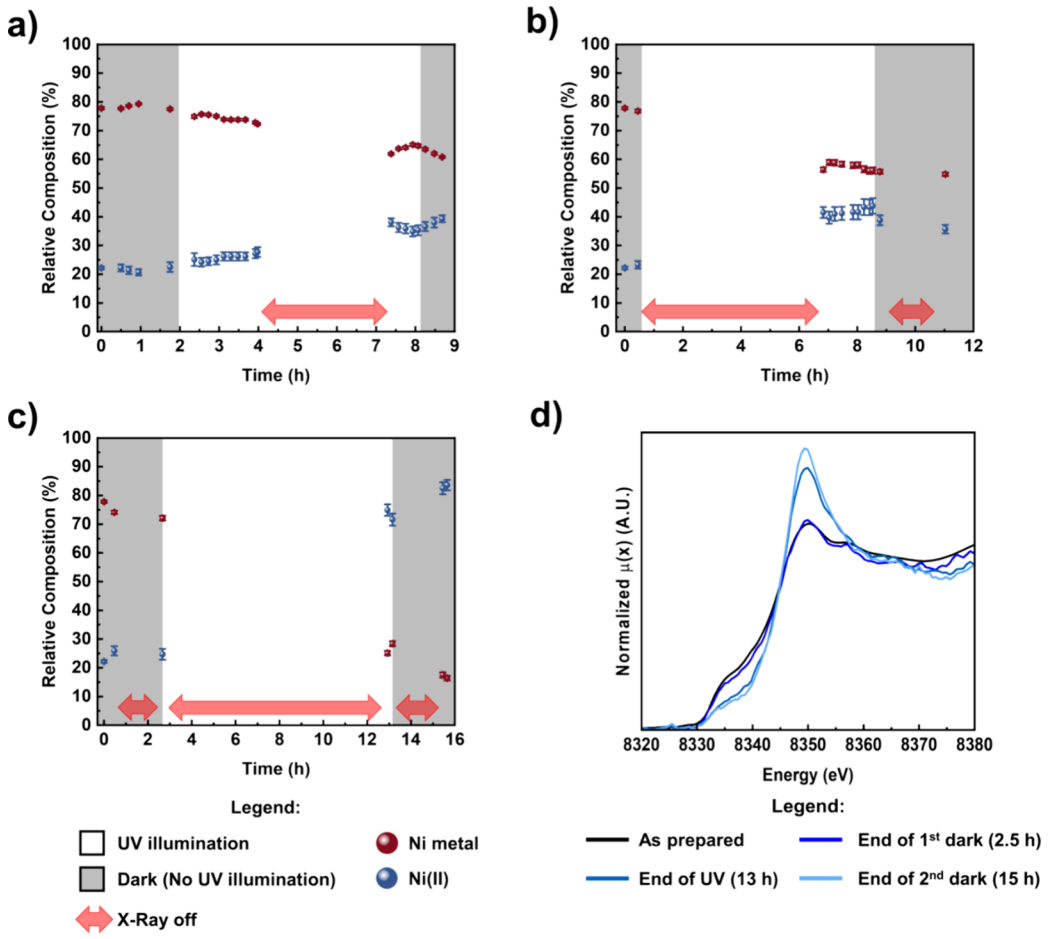

Figure 6. (a−c) Fitting results of in situ XANES spectra of Ni-STO with reduced exposure of the photocatalyst slurry to the probing X-ray beam. The data at $t = 0$ refer to the ex-situ XANES measurements of as-prepared Ni-STO; gray areas represent data points acquired under dark conditions, while white areas refer to data points acquired under UV illumination, and red arrows refer to the absence of X-ray (X-ray shutter closed). In (b), the exposure time to UV light amounts to ∼4 h, while in (c), the exposure time to UV light amounts to ∼10 h. (d) Selected, normalized Ni K-edge XANES spectra of Ni-STO for experiment (c).

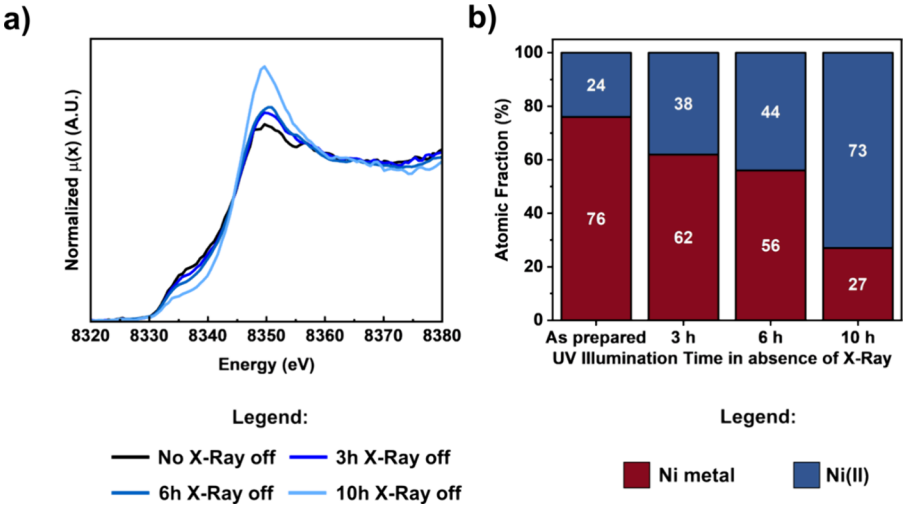

Figure 7. (a) Normalized Ni K-edge in situ spectra for different UV irradiation times in the absence of the X-ray probing beam. (b) Ni(0) and Ni(II) atomic fraction obtained by fitting the spectra in (a).

However, clear changes in the Ni oxidation state take place under UV illumination, as shown in Figure 6a−c, where each plot represents a single batch experiment. For example, the experiment in Figure 6a shows that after ca. 2 h of UV illumination with continuous X-ray exposure, minor but sizable changes in the Ni(0) and Ni(II) atomic fractions can be detected, well in line with data in Figure 5. However, when the photocatalyst is kept for another 3 h of UV illumination in the

https://doi.org/10.1021/acs.jpcc.4c04688
J. Phys. Chem. C XXXX, XXX, XXX−XXX

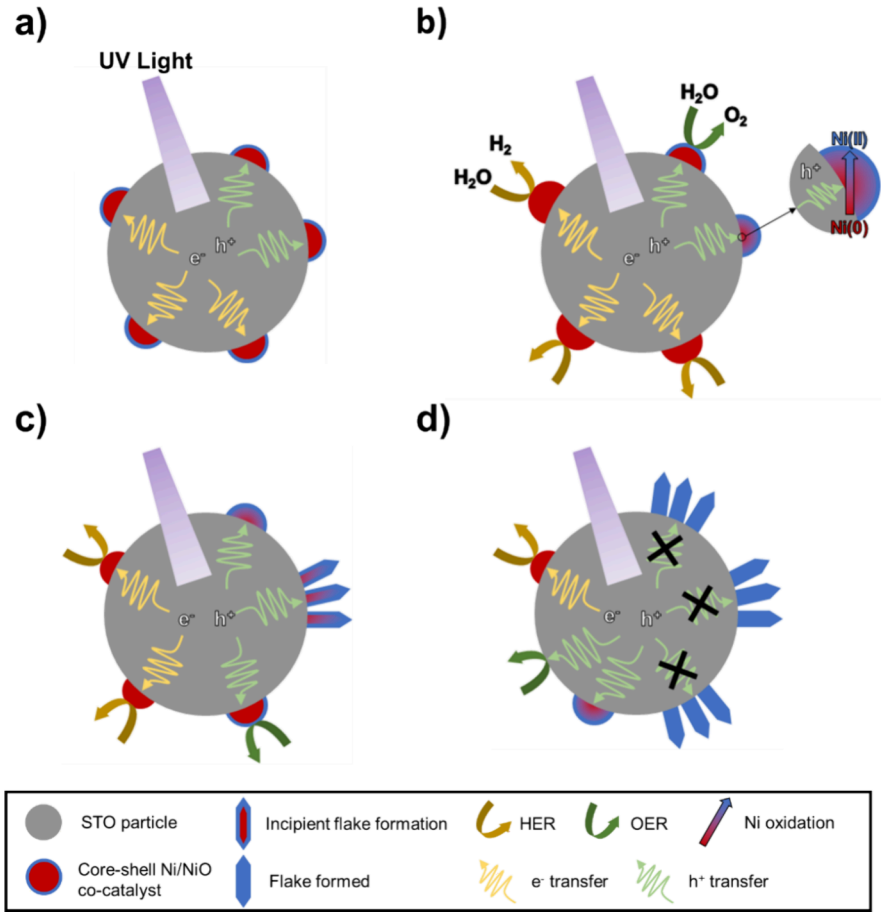

Figure 8. Schematic representation of the photocatalyst deactivation: (a) as-prepared photocatalyst and charge carrier generation upon UV excitation; (b) photocatalyzed HER, OER, and Ni oxidation to Ni(II); (c) restructuring of Ni cocatalyst; (d) partially deactivated photocatalyst after prolonged UV illumination.

absence of X-ray exposure, the oxidation of Ni becomes even more noticeable, as the Ni(0):Ni(II) ratio decreases from 4 (80% Ni(0), 20% Ni(II)) to about 1.5 (60% Ni(0), 40% Ni(II))—shown in Figure 6b. Furthermore, Figure 6c demonstrates that extending the UV exposure time (in the absence of X-ray) leads to an inversion of the ratio of Ni(0):Ni(II) from 4 to 0.25, i.e., prolonged UV irradiation leads to further oxidation of the remainder Ni phase in the cocatalyst.

Figure 6d shows the XANES spectra after each light on−off cycle with minimized X-ray exposure of the suspension for the experiment in Figure 6c (10 h-long UV irradiation performed completely in the absence of X-ray exposure). The dramatic increase in the intensity of the white line in the Ni K-edge XANES spectra after UV illumination proves the formation of large amounts of oxidized nickel phases (solid NiO and $Ni(OH)_2$). This correlates well with the results of ex-situ XPS, showing that the content of the $Ni(OH)_2$ phase increases after photocatalysis. The quantitative difference in phase compositions from the two techniques (XAS vs XPS) can be explained by considering that XAS is a bulk technique, thus probing the entirety of the cocatalyst NPs. On the contrary, XPS is surface-sensitive (with an average penetration depth of a few nanometers), and hence, it allows to probe only the photocatalyst surface.

We show in Figure 7a in situ spectra measured at the end of the UV illumination period for different experiments carried out by systematically reducing the photocatalyst exposure to the probing beam under UV illumination (from continuous to no X-ray exposure). Figure 7b summarizes the results of the different in situ XAS experiments outlined in Figure S6 and Figure 6—indicating the Ni(0) and Ni(II) percentages after variable UV exposure time. Once more, it is evident that the shorter the exposure of the photocatalyst slurry to the probing X-ray beam, the more prominent the Ni oxidation. Taking the substoichiometric H_2:O_2 ratio into consideration, the Ni(0)/Ni(II) composition change can be explained by the oxidation of Ni(0) to Ni(II) phases by photogenerated holes (eq 5).

$$Ni_{(s)} + 2h^+_{VB} + H_2O_{(l)} \rightarrow NiO_{(s)} + 2H^+_{(aq)} \quad (5)$$

We propose that under UV illumination, metallic Ni sites trap and transfer photogenerated electrons to water, leading to H_2 formation. Hence, in agreement with our earlier work,[15] metallic Ni is the active phase responsible for hydrogen evolution—in contrast to that proposed in other previous studies.[16,27,31] At the same time, other Ni sites (particles) are partially oxidized to NiO by photogenerated holes (i.e., h^+ oxidizes Ni instead of H_2O, eq 5), which results in a decrease of the hydrogen production rate over time (Figure 2b). The outer layer of the NiO phase produced under illumination is then hydrated, leading to the formation of a $Ni(OH)_2$ phase (eq 6).

$$NiO_{(s)} + H_2O_{(l)} \rightarrow Ni(OH)_{2(s)} \quad (6)$$

https://doi.org/10.1021/acs.jpcc.4c04688
J. Phys. Chem. C XXXX, XXX, XXX−XXX

Finally, taking into account that Ni does not leach out from the photocatalyst (based on XPS and ICP-MS analyses), we considered the possibility that a dynamic equilibrium takes place under UV illumination where metallic Ni is oxidized by STO VB holes to soluble Ni(II) species. Such $Ni(II)_{(aq)}$ species can then be either photoreduced by CB electrons to Ni, depositing onto the STO surface (i.e., photodeposition), or form $Ni(OH)_2$ due to a local, relatively high pH.

Photodeposition of metal cocatalyst NPs on various photocatalysts under UV irradiation is well documented in the literature[40−42] but typically requires a hole scavenger (e.g., methanol and ethanol).[43,44]

To test this possibility,[23] we performed in situ XAS experiments with pristine STO powders suspended in DI water and in the presence of a dissolved Ni(II) salt (10 mM $NiSO_4$ aqueous solution). Also in this case, we aimed at minimizing the exposure of the slurry to the probing beam, and hence, in situ XANES spectra were acquired only twice during the experiment, i.e., in the dark before starting UV illumination and directly after 4 h of UV irradiation. These spectra are shown in Figure S9, along with a reference spectrum of a $NiSO_4$ aqueous solution taken in the absence of the STO photocatalyst. The in situ spectra for the STO slurry are identical before and after UV illumination and feature the same spectral shape of the reference $NiSO_4$ aqueous solution. Thus, we can rule out the possibility of Ni^{2+} photoreduction to Ni(0) onto STO. Furthermore, GC analysis of the gas headspace (Figure S10) shows that the addition of the Ni(II) salt to the reaction medium does not lead to any increase of the H_2 evolution rate but it rather has a detrimental effect on the photocatalytic H_2 evolution rate of pristine STO. This result might be explained by the fact that solvated Ni(II) ions absorb UV photons, and hence attenuate the photon flux reaching STO.

To conclude, we sketch in Figure 8 the proposed mechanisms for photocatalyst water splitting and deactivation based on the results of in situ and ex-situ characterization techniques discussed above.

In the as-prepared state (Figure 8a), the Ni cocatalyst is in the form of Ni/Ni(II) core−shell NPs, with a Ni(0):Ni(II) at % ratio of approximately 4. Upon illumination, due to the interaction between (coupling of) the STO and the Ni NPs, charge carriers photogenerated in the STO can transfer to the Ni cocatalysts. We propose that in the early stage of UV illumination (Figure 8b), a portion of the Ni core−shell NPs can trap CB electrons and undergo reduction to the Ni(0) phase, according to the NiO (Ni^{2+})/Ni (Ni^0) equilibrium potential at pH 7[45] and the CB edge of STO (exit energy of CB electrons). Thus, the metallic Ni phase is the active site for water reduction, thus catalyzing HER. At the same time, VB holes can also transfer to cocatalyst NPs. Such holes can either be transferred to water, thus catalyzing the OER, or react with the Ni(0) phase, leading to Ni(0) oxidation. In the latter case, the oxidized Ni particles undergo morphological restructuring into a flake-like morphology (Figure 8c,d). By increasing the UV illumination time (Figure 8d), more core−shell particles are transformed into Ni oxide flake-like structures, which are inactive for water splitting. Different TEM and SEM images were taken for the same sample after photocatalysis for 6 h; see Figure S11. The different size of the flakes and morphology of the NPs provide evidence for the dynamic nature of the Ni-STO photocatalyst and can be ascribed to different stages of Ni oxidation. Eventually, this leads to water oxidation taking place at low rates (likely onto the bare STO surface), while some reduced cocatalyst particles keep acting as the H_2 evolution site (Figure 8d).

Future studies should investigate the regeneration of the deactivated photocatalyst, e.g., by thermal treatment in reducing atmospheres, to reduce the high oxidation states of Ni to a metallic phase needed for hydrogen evolution. Even more desirable is to identify ways to avoid Ni oxidation. To achieve this, a possible strategy could be to deposit OER and HER cocatalysts on hole and electron-collecting facets, respectively, of the supporting semiconductor—a concept so far demonstrated only for noble metal-based cocatalysts—[46−48] while for earth-abundant cocatalysts, stability issues remain a concern.

Finally, we investigated the effect of hole scavengers on the Ni-STO-photoinduced degradation. Adding hole scavengers, such as MeOH and EtOH, to the reaction medium is a common strategy to reduce the e^-−h^+ recombination rate, thus improving the photocatalyst performance in terms of hydrogen evolution rate.[49,50] The data in Figure S12a show a significant improvement in the photocatalytic H_2 evolution performance of the Ni-STO photocatalyst when MeOH is added to the solution as a hole scavenger. In a previous work, in situ XAS techniques were used to demonstrate the photoreduction of oxidized Ni phases (e.g., NiO) to metallic Ni (Ni^0) on TiO_2 photocatalysts in the presence of EtOH as a hole scavenger under UV illumination.[29] The data in Figure S12a reveal a significantly higher and more stable hydrogen evolution rate (maximum value of 375 μmol h^{-1} g^{-1} compared to 50 μmol h^{-1} g^{-1}) during a few hours of high photon flux UV illumination, confirming that (i) in the presence of a hole scavenger, the metallic Ni phase undergoes oxidation to a minor extent, hence sustaining a higher and almost constant H_2 generation rate over time—in other words, inhibiting Ni oxidation increases the H_2 generation rate; while (ii) in the absence of a hole scavenger, VB holes are responsible for Ni oxidation and for the degradation of the Ni-STO photocatalytic activity. Figure S12b,c shows an SEM image of the used Ni-STO photocatalyst tested in a methanol−water solution. The data indicate that the morphology of the Ni cocatalyst NPs remains unaltered compared to the as-prepared photocatalyst.

Interestingly, the schematic shown in Figure 8 is different from the structural changes proposed by Han and co-workers.[15] Two differences should be noted in comparing the two studies, which are the following: (i) the sample was not exposed to a mild oxidation in air at 200 °C but carefully exposed to ambient conditions after thermal reduction, which might lead to a less conformal oxide shell coverage and a thinner oxide shell thickness, and (ii) the UV-light intensity used here was significantly higher than applied in the previous study.[15] Future research should address the effect of the $NiO/Ni(OH)_2$ shell thickness and illumination intensity on the performance and degradation of Ni-$SrTiO_3$ photocatalysts in overall water splitting.

CONCLUSIONS

In the present work, we used in situ XAS techniques to investigate the deactivation mechanism of a nanostructured Ni−STO photocatalyst for water splitting. We devised a liquid-phase spectroscopic cell for XAS measurements in fluorescence mode to monitor changes in the Ni cocatalyst oxidation state during photocatalytic H_2 generation from photocatalyst suspensions in plain water. Continuous exposure of the photocatalyst to X-ray illumination was found to prevent the in situ oxidation of Ni during UV illumination. To overcome this effect (i.e., the undesired beam induced effect, likely due to photolysis of

https://doi.org/10.1021/acs.jpcc.4c04688
J. Phys. Chem. C XXXX, XXX, XXX−XXX

water), we carried out a series of in situ XAS experiments by systematically reducing the exposure of the UV-illuminated photocatalyst suspension to the probing beam. We demonstrated that the instability of the Ni cocatalyst is due to its oxidation and reconstruction, to Ni(II) species, caused by photogenerated VB holes. We concluded that this phenomenon is the root cause of the poor durability of Ni-STO water splitting photocatalysts. We also ruled out dissolution of Ni in the form of solvated Ni(II) species as well as photodeposition of solvated Ni(II) ions (via photoreduction) onto the photocatalyst surface.

■ ASSOCIATED CONTENT

Supporting Information

The Supporting Information is available free of charge at https://pubs.acs.org/doi/10.1021/acs.jpcc.4c04688.

Additional experimental details, and photocatalytic, XAS, ICP-MS, TEM, and SEM data (PDF)

■ AUTHOR INFORMATION

Corresponding Author

Marco Altomare − *Department of Chemical Engineering, MESA+ Institute for Nanotechnology, University of Twente, Enschede 7500 AE, The Netherlands;* orcid.org/0000-0002-7237-8809; Email: m.altomare@utwente.nl

Authors

MemetTursun Abudukade − *Department of Chemical Engineering, MESA+ Institute for Nanotechnology, University of Twente, Enschede 7500 AE, The Netherlands*

Marco Pinna − *Department of Chemical Engineering, MESA+ Institute for Nanotechnology, University of Twente, Enschede 7500 AE, The Netherlands; Department of Science and High Technology, University of Insubria, Como 22100, Italy; Dipartimento di Chimica, Università degli Studi di Milano, Milan 20133, Italy;* orcid.org/0000-0003-3787-9920

Davide Spanu − *Department of Science and High Technology, University of Insubria, Como 22100, Italy;* orcid.org/0000-0001-7948-2839

Giuditta De Amicis − *Dipartimento di Chimica, Università degli Studi di Pavia, Pavia 27100, Italy*

Alessandro Minguzzi − *Dipartimento di Chimica, Università degli Studi di Milano, Milan 20133, Italy; UdR INSTM di Milano - Consorzio Interuniversitario Nazionale per la Scienza e Tecnologia dei Materiali − INSTM, Firenze 50121, Italy;* orcid.org/0000-0002-8130-4465

Alberto Vertova − *Dipartimento di Chimica, Università degli Studi di Milano, Milan 20133, Italy; UdR INSTM di Milano - Consorzio Interuniversitario Nazionale per la Scienza e Tecnologia dei Materiali − INSTM, Firenze 50121, Italy;* orcid.org/0000-0003-3858-9730

Sandro Recchia − *Department of Science and High Technology, University of Insubria, Como 22100, Italy;* orcid.org/0000-0002-4865-5757

Paolo Ghigna − *Dipartimento di Chimica, Università degli Studi di Pavia, Pavia 27100, Italy;* orcid.org/0000-0002-8680-7272

Guido Mul − *Department of Chemical Engineering, MESA+ Institute for Nanotechnology, University of Twente, Enschede 7500 AE, The Netherlands;* orcid.org/0000-0001-5898-6384

Complete contact information is available at: https://pubs.acs.org/10.1021/acs.jpcc.4c04688

Author Contributions

#M.A. and M.P. have equal contributions.

Notes

The authors declare no competing financial interest.

■ ACKNOWLEDGMENTS

This research was financially supported by the Deutsche Forschungsgemeinschaft DFG (project no. DFG-grant AL 2479/1-1) and the Nederlandse Organisatie voor Wetenschappelijk Onderzoek NWO (project no. ECCM.TT.ECCM.005). We acknowledge the Deutsches Elektronen-Synchrotron (DESY) for provision of synchrotron radiation facilities using beamline P65 (DOI: 10.1063/1.5084603) and Dr. Edmund Welter for technical assistance in using the beamline. We acknowledge the Italian ELETTRA Synchrotron for provision of synchrotron facilities using beamline XAFS (DOI: 10.1088/1742-6596/190/1/012043) and Dr. Luca Olivi, Dr. Giovanni Agostini, and Mr. Riccardo Grisonich for technical support during the beamtime. The authors would also like to acknowledge Dr. Kai Han (Shell plc), Prof. Dr. Bastian Mei (Ruhr University Bochum), and Robert Meijer (PCS, University of Twente) for technical support with the GC setup, Prof. Dr. Wiebe de Vos and the MST group at the University of Twente for the SEM analysis, Dr. Martina Tsvetanova and Dr. Yibin Bu (Nanolab, University of Twente, MESA+ Institute for Nanotechnology) for the TEM (and TEM−EDX) and XPS analysis, respectively.

■ REFERENCES

(1) Fox, M. A.; Dulay, M. T. Heterogeneous Photocatalysis. *Chem. Rev.* **1993**, *93* (1), 341−357.

(2) Kudo, A.; Miseki, Y. Heterogeneous Photocatalyst Materials for Water Splitting. *Chem. Soc. Rev.* **2009**, *38* (1), 253−278.

(3) Altomare, M.; Nguyen, N. T.; Naldoni, A.; Marschall, R. Structure, Materials, and Preparation of Photoelectrodes. *Photoelectrocatalysis: Fundamentals and Applications* **2023**, 83−174.

(4) Wenderich, K.; Altomare, M.; Cremades, A.; Maestre, D. Metal Oxide Semiconductor Nanomaterials for Heterogeneous Photocatalysis. *Sustainable Nanomater. Energy Appl.* **2023**, *6*, 6-1−6-71.

(5) Kanhere, P.; Chen, Z. Molecules A Review on Visible Light Active Perovskite-Based Photocatalysts. *Molecules* **2014**, *19* (12), 19995−20022.

(6) Wang, Q.; Domen, K. Particulate Photocatalysts for Light-Driven Water Splitting: Mechanisms, Challenges, and Design Strategies. *Chem. Rev.* **2020**, *120*, 919−985.

(7) Altomare, M.; Nguyen, N. T.; Schmuki, P. Templated Dewetting: Designing Entirely Self-Organized Platforms for Photocatalysis. *Chem. Sci.* **2016**, *7* (12), 6865−6886.

(8) Maeda, K.; Teramura, K.; Lu, D.; Takata, T.; Saito, N.; Inoue, Y.; Domen, K. Photocatalyst Releasing Hydrogen from Water. *Nature* **2006**, *440* (7082), 295−295.

(9) Gomes Silva, C.; Juárez, R.; Marino, T.; Molinari, R.; García, H. Influence of Excitation Wavelength (UV or Visible Light) on the Photocatalytic Activity of Titania Containing Gold Nanoparticles for the Generation of Hydrogen or Oxygen from Water. *J. Am. Chem. Soc.* **2011**, *133* (3), 595−602.

(10) Sayed, F. N.; Jayakumar, O. D.; Sasikala, R.; Kadam, R. M.; Bharadwaj, S. R.; Kienle, L.; Schürmann, U.; Kaps, S.; Adelung, R.; Mittal, J. P.; et al. Photochemical Hydrogen Generation Using Nitrogen-Doped TiO_2 − Pd Nanoparticles: Facile Synthesis and Effect of Ti^{3+} Incorporation. *J. Phys. Chem. C* **2012**, *116* (23), 12462−12467.

(11) Tran, P. D.; Xi, L.; Batabyal, S. K.; Wong, L. H.; Barber, J.; Chye Loo, J. S. Enhancing the Photocatalytic Efficiency of TiO2 Nanopowders for H2 Production by Using Non-Noble Transition Metal Co-Catalysts. *Phys. Chem. Chem. Phys.* **2012**, *14* (33), 11596.

(12) Pinna, M.; Wei, A. W. W.; Spanu, D.; Will, J.; Yokosawa, T.; Spiecker, E.; Recchia, S.; Schmuki, P.; Altomare, M. Amorphous NiCu Thin Films Sputtered on TiO2 Nanotube Arrays: A Noble-Metal Free Photocatalyst for Hydrogen Evolution. *ChemCatChem.* **2022**, *14* (23), No. e202201052.
(13) Lin, J.-D.; Yan, S.; Huang, Q.-D.; Fan, M.-T.; Yuan, Y.-Z.; Tan, T. T.-Y.; Liao, D.-W. TiO2 Promoted by Two Different Non-Noble Metal Cocatalysts for Enhanced Photocatalytic H2 Evolution. *Appl. Surf. Sci.* **2014**, *309*, 188−193.
(14) Liu, J.; Jia, Q.; Long, J.; Wang, X.; Gao, Z.; Gu, Q. Amorphous NiO as Co-Catalyst for Enhanced Visible-Light-Driven Hydrogen Generation over g-C 3 N 4 Photocatalyst. *Appl. Catal., B* **2018**, *222*, 35−43.
(15) Han, K.; Kreuger, T.; Mei, B.; Mul, G. Transient Behavior of Ni@ NiO $_x$ Functionalized SrTiO $_3$ in Overall Water Splitting. *ACS Catal.* **2017**, *7* (3), 1610−1614.
(16) Zhang, L.; Liu, Q.; Aoki, T.; Crozier, P. A. Structural Evolution during Photocorrosion of Ni/NiO Core/Shell Cocatalyst on TiO $_2$. *J. Phys. Chem. C* **2015**, *119* (13), 7207−7214.
(17) Townsend, T. K.; Browning, N. D.; Osterloh, F. E. Overall Photocatalytic Water Splitting with NiOx−SrTiO3 − a Revised Mechanism. *Energy Environ. Sci.* **2012**, *5* (11), 9543.
(18) Dutta, A.; Appel, A. M.; Shaw, W. J. Designing Electrochemically Reversible H2 Oxidation and Production Catalysts. *Nat. Rev. Chem.* **2018**, *2* (9), 244−252.
(19) Shotonwa, I. O.; Ejeromedoghene, O.; Adesoji, A. O.; Adewuyi, S. Electrochemistry and Electrocatalysis of H2 Generation Using Hexacoordinated Nickel—Based Complexes. *Catal. Commun.* **2023**, *179*, No. 106680.
(20) Friebel, D.; Louie, M. W.; Bajdich, M.; Sanwald, K. E.; Cai, Y.; Wise, A. M.; Cheng, M. J.; Sokaras, D.; Weng, T. C.; Alonso-Mori, R.; et al. Identification of Highly Active Fe Sites in (Ni,Fe)OOH for Electrocatalytic Water Splitting. *J. Am. Chem. Soc.* **2015**, *137* (3), 1305−1313.
(21) Trotochaud, L.; Young, S. L.; Ranney, J. K.; Boettcher, S. W. Nickel-Iron Oxyhydroxide Oxygen-Evolution Electrocatalysts: The Role of Intentional and Incidental Iron Incorporation. *J. Am. Chem. Soc.* **2014**, *136* (18), 6744−6753.
(22) Domen, K. Mechanism of Photocatalytic Decomposition of Water into H2 and O2 over NiO$z.Sbnd;SrTiO3. *J. Catal.* **1986**, *102* (1), 92−98.
(23) Domen, K.; Naito, S.; Onishi, T.; Tamaru, K. Photocatalytic Decomposition of Liquid Water on a NiO—SrTiO3 Catalyst. *Chem. Phys. Lett.* **1982**, *92* (4), 433−434.
(24) Domen, K.; Kudo, A.; Onishi, T.; Kosugi, N.; Kuroda, H. Photocatalytic Decomposition of Water into H2 and O2 over NiO-SrTiO3 Powder. 1. Structure of the Catalyst. *J. Phys. Chem.* **1986**, *90* (2), 292−295.
(25) Domen, K.; Naito, S.; Onishi, T.; Tamaru, K.; Soma, M. Study of the Photocatalytic Decomposition of Water Vapor over a NiO-SrTiO3 Catalyst. *J. Phys. Chem.* **1982**, *86* (18), 3657−3661.
(26) Domen, K.; Naito, S.; Soma, M.; Onishi, T.; Tamaru, K. Photocatalytic Decomposition of Water Vapour on an NiO−SrTiO3 Catalyst. *J. Chem. Soc. Chem. Commun.* **1980**, *12*, 543−544.
(27) Baba, R.; Fujishima, A. Where Is the Actual Site for Hydrogen Evolution? *J. Electroanal Chem. Interfacial Electrochem* **1986**, *213* (2), 319−321.
(28) Han, K.; Haiber, D. M.; Knöppel, J.; Lievens, C.; Cherevko, S.; Crozier, P.; Mul, G.; Mei, B. CrO $_x$ -Mediated Performance Enhancement of Ni/NiO-Mg:SrTiO $_3$ in Photocatalytic Water Splitting. *ACS Catal.* **2021**, *11* (17), 11049−11058.
(29) Spanu, D.; Minguzzi, A.; Recchia, S.; Shahvardanfard, F.; Tomanec, O.; Zboril, R.; Schmuki, P.; Ghigna, P.; Altomare, M. An Operando X-Ray Absorption Spectroscopy Study of a NiCu−TiO $_2$ Photocatalyst for H $_2$ Evolution. *ACS Catal.* **2020**, *10* (15), 8293−8302.
(30) Altomare, M.; Qin, S.; Saveleva, V. A.; Badura, Z.; Tomanec, O.; Mazare, A.; Zoppellaro, G.; Vertova, A.; Taglietti, A.; Minguzzi, A.; et al. Metastable Ni(I)-TiO $_{2-x}$ Photocatalysts: Self-Amplifying H $_2$ Evolution from Plain Water without Noble Metal Co-Catalyst and Sacrificial Agent. *J. Am. Chem. Soc.* **2023**, *145* (48), 26122−26132.
(31) Domen, K.; Kudo, A.; Onishi, T.; Kosugi, J. N.; Kuroda, H. Photocatalytic Decomposition of Water into H2 and 02 over NiO-SrTi03 Powder. 1. Structure of the Catalyst. *J. Phys. Chem.* **1986**, *90*, 292−295.
(32) Monticelli, D.; Castelletti, A.; Civati, D.; Recchia, S.; Dossi, C. How to Efficiently Produce Ultrapure Acids. *Int. J. Anal Chem.* **2019**, *2019*, 1.
(33) Han, K. *Photocatalytic Overall Water Splitting Using Modified SrTiO$_3$*. University of Twente 2018, DOI: .
(34) Ravel, B.; Newville, M. ATHENA, ARTEMIS, HEPHAESTUS: Data Analysis for X-Ray Absorption Spectroscopy Using IFEFFIT. *Journal of Synchrotron Radiation* **2005**, *12*, 537−541.
(35) Le, M. V.; Vo, N. Q. D.; Le, Q. C.; Tran, V. A.; Phan, T. Q. P.; Huang, C. W.; Nguyen, V. H. Manipulating the Structure and Characterization of Sr1−xLaxTiO3 Nanocubes toward the Photodegradation of 2-Naphthol under Artificial Solar Light. *Catalysts* **2021**, *11*, 564.
(36) Agrawal, A.; Habibi, H. R.; Agrawal, R. K.; Cronin, J. P.; Roberts, D. M.; Caron-Popowich, R.; Lampert, C. M. Effect of Deposition Pressure on the Microstructure and Electrochromic Properties of Electron-Beam-Evaporated Nickel Oxide Films. *Thin Solid Films* **1992**, *221* (1−2), 239−253.
(37) Li, W.; Yang, J.; Isimjan, T. T.; Yang, D.-Q.; Sacher, E. Aqueous Synthesis and Growth of Morphologically Controllable, Hierarchical Ni(OH) $_2$ Nanostructures. *Mater. Res. Express* **2015**, *2* (7), No. 075011.
(38) Biesinger, M. C.; Payne, B. P.; Grosvenor, A. P.; Lau, L. W. M.; Gerson, A. R.; Smart, R. St. C. Resolving Surface Chemical States in XPS Analysis of First Row Transition Metals, Oxides and Hydroxides: Cr, Mn, Fe, Co and Ni. *Appl. Surf. Sci.* **2011**, *257* (7), 2717−2730.
(39) Greczynski, G.; Hultman, L. X-Ray Photoelectron Spectroscopy: Towards Reliable Binding Energy Referencing. *Prog. Mater. Sci.* **2020**, *107*, No. 100591.
(40) Zhan, D.; Tian, J.; Fu, Q.; Liu, P.; Zhao, Y.; Liu, W.; Li, D.; Huang, Y.; Han, C. In Situ Photodeposition of Cu and Ni(OH)2 Dual Cocatalyst: Synergistic Effect on Enhancing g-C3N4 Photocatalytic H2 Evolution. *Appl. Surf. Sci.* **2023**, *641*, No. 158463.
(41) Cebada, S.; Soto, E.; Mota, N.; García Fierro, J. L.; Navarro, R. M. Effect of Photodeposition Conditions on Ni−CdS Photocatalysts and Its Role in the Photoactivity for H2 Production from Ethanolic Solutions. *Int. J. Hydrogen Energy* **2020**, *45* (40), 20536−20548.
(42) Wenderich, K.; Mul, G. Methods, Mechanism, and Applications of Photodeposition in Photocatalysis: A Review. *Chem. Rev.* **2016**, *116* (23), 14587−14619.
(43) Wang, W.; Liu, S.; Nie, L.; Cheng, B.; Yu, J. Enhanced Photocatalytic H $_2$ -Production Activity of TiO $_2$ Using Ni(NO $_3$) $_2$ as an Additive. *Phys. Chem. Chem. Phys.* **2013**, *15* (29), 12033−12039.
(44) Forouzan, F.; Richards, T. C.; Bard, A. J. Photoinduced Reaction at TiO $_2$ Particles. Photodeposition from Ni ^{II} Solutions with Oxalate. *J. Phys. Chem.* **1996**, *100* (46), 18123−18127.
(45) Huang, L.-F.; Hutchison, M. J.; Santucci, R. J.; Scully, J. R.; Rondinelli, J. M. Improved Electrochemical Phase Diagrams from Theory and Experiment: The Ni−Water System and Its Complex Compounds. *J. Phys. Chem. C* **2017**, *121* (18), 9782−9789.
(46) Li, R.; Han, H.; Zhang, F.; Wang, D.; Li, C. Highly Efficient Photocatalysts Constructed by Rational Assembly of Dual-Cocatalysts Separately on Different Facets of BiVO4. *Energy Environ. Sci.* **2014**, *7* (4), 1369−1376.
(47) Ding, J.; Li, X.; Chen, L.; Zhang, X.; Yin, H.; Tian, X. Site-Selective Deposition of Reductive and Oxidative Dual Cocatalysts to Improve the Photocatalytic Hydrogen Production Activity of CaIn 2 S 4 with a Surface Nanostep Structure. *ACS Appl. Mater. Interfaces* **2019**, *11* (1), 835−845.
(48) Mu, L.; Zhao, Y.; Li, A.; Wang, S.; Wang, Z.; Yang, J.; Wang, Y.; Liu, T.; Chen, R.; Zhu, J.; Fan, F.; Li, R.; Li, C. Enhancing Charge Separation on High Symmetry SrTiO3 Exposed with Anisotropic Facets for Photocatalytic Water Splitting. *Energy Environ. Sci.* **2016**, *9* (7), 2463−2469.

https://doi.org/10.1021/acs.jpcc.4c04688
J. Phys. Chem. C XXXX, XXX, XXX−XXX

(49) López, C. R.; Melián, E. P.; Méndez, J. A. O.; Santiago, D. E.; Doña Rodríguez, J. M.; Díaz, O. G. Comparative Study of Alcohols as Sacrificial Agents in H 2 Production by Heterogeneous Photocatalysis Using Pt/TiO 2 Catalysts. *J. Photochem. Photobiol. A* **2015**, *312*, 45−54.
(50) Shahvaranfard, F.; Ghigna, P.; Minguzzi, A.; Wierzbicka, E.; Schmuki, P.; Altomare, M. Dewetting of PtCu Nanoalloys on TiO2Nanocavities Provides a Synergistic Photocatalytic Enhancement for Efficient H2Evolution. *ACS Appl. Mater. Interfaces* **2020**, *12* (34), 38211−38221.

https://doi.org/10.1021/acs.jpcc.4c04688
J. Phys. Chem. C XXXX, XXX, XXX−XXX